Electronic Supplementary Material (ESI) for Journal of Materials Chemistry A.

Strain relaxation and domain enlargement via phase transition towards efficient $CsPbI_2Br$ solar cells

Fa-Zheng Qiu,[a,b 1] Ming-Hua Li,[a 1] Shuo Wang,[a] Yan Jiang,[c]* Jun-Jie Qi,[b]* and Jin-Song Hu[a,d]*

[a] Beijing National Laboratory for Molecular Sciences (BNLMS), CAS Key Laboratory of Molecular Nanostructure and Nanotechnology, Institute of Chemistry, Chinese Academy of Sciences, Beijing 100190, China.

[b] School of Materials Science and Engineering, University of Science and Technology Beijing, Beijing 100083, China.

[c] Energy Materials and Optoelectronics Unit, Songshan Lake Materials Laboratory, Dongguan, Guangdong 523808, China.

[d] School of Chemical Sciences, University of Chinese Academy of Sciences, Beijing 100049, China.

Experimental Section

Chemicals: Lead iodide (PbI_2, 99.999 %), lead bromide ($PbBr_2$, 99.999 %), Cesium iodide (CsI, 99.999 %), Chlorobenzene (CB, 99.9 %), and dimethyl sulfoxide (DMSO, ≥ 99.9 %) were purchased from Sigma-Aldrich. SnO_2 dispersion (15 wt% in H_2O) was purchased from Alfa Aesar. Poly(3-hexylthiophene) (P3HT) was purchased from Xi'an Polymer Light Technology in China. All of the purchased chemicals were used as received without further purification.

Precursor Solution Preparation: The SnO_2 precursor solution was prepared according to a formula (V (SnO_2 dispersion): V (H_2O): V (isopropyl alcohol) = 1: 3: 3). The $CsPbI_2Br$ precursor solution (1.2 M) was prepared by dissolving CsI (1.2 M), PbI_2 (0.6 M) and $PbBr_2$ (0.6 M) in DMSO, which was stirred at 60 °C for about 2 hours in a N_2 glovebox. The P3HT solution was prepared by dissolving P3HT (10 mg) in 1 mL of CB solution.

Device Fabrication: The prepared precursor solution was filtered before utilization. The pre-patterned ITO substrates (15 Ω sq^{-1}) were ultrasonically cleaned by using water, ethanol, acetone, and isopropyl alcohol in an ultrasonic bath sequentially, and then treated with UV-ozone for 10 min. The compact SnO_2 layer was spin-coated on the substrates at 3000 rpm for 15 s, followed by annealing at 150 °C for 15 min in ambient air. Next, the $CsPbI_2Br$ precursor solutions were spin-coated onto the compact SnO_2 layer via a two-step process. The first step was 1000 rpm for 10 s, and the second step was 2000 rpm for 120 s. Subsequently, the films were annealed at 50 °C for 2 min and at 160 °C for 10 min. For the PTG films, the prepared $CsPbI_2Br$ films accomplished phase conversion (α phase→δ phase) at 80 % humidity. After that, the δ-phase $CsPbI_2Br$ films were annealed again at 280 ℃ for 10 min to obtain the α phase. The P3HT solution was spin-coated on perovskite

at 3000 rpm for 30 s. Finally, 80 nm of Au was thermally evaporated as a top electrode using a shadow mask. The active device area was 0.24 cm^2. When measuring, a 0.1 cm^2 non-reflective mask was used to define the accurate area. The $CsPbI_2Br$ powder obtained by scraping the as-prepared perovskite films from substrates.

Characterization: Out-of-plane X-ray diffraction (XRD) patterns were obtained on a Regaku D/Max-2500 diffractometer equipped with a Cu Kα1 radiation (λ = 1.5406 Å). In-plane XRD measurements were carried out with the Rigaku SmartLab diffractometer using Cu Ka radiation (λ = 1.5406 Å, Rigaku, Japan). Scanning electron microscopy (SEM) was performed on Hitachi S-4800. The surface roughness of perovskite film was measured by an AFM (Nanoscope V, Vecco) at tapping mode. The ultraviolet-visible (UV-vis) absorption spectra were collected on a UV-vis spectrophotometer (UH4150, Hitachi). The steady-state PL and TRPL spectra were measured in an Edinburgh Instrument FLS 980. J-V curves were measured using a solar simulator (450 W Model 94023A, Newport) with an AM 1.5 solar spectrum filter and a Keithley 2420 source meter. Light intensity was adjusted using a NREL certified Si solar cell. The external quantum efficiency (EQE) spectra were measured with the ORIEL IQE-200.

Supplementary Note 1: The relationship between in-plane strain and out-of-plane strain

If there is a compressive strain in perovskite film along the out-of-plane direction (ε_y), the in-plane direction (ε_x) would be under the tensile strain simultaneously, and vice versa.[1] Moreover, ε_x and ε_y are linearly related according to the Poisson's ratio Equation S1.

$$\varepsilon_y = -\upsilon\varepsilon_x \qquad \text{Equation S1}$$

where ε_y is compressive strain of the out-of-plane, ε_x is tensile strain of the in-plane, and υ is Poisson's ratio.

Supplementary Note 2: Strain calculation and discussion

When a perovskite film is deposited on a substrate with a much smaller thermal expansion coefficient, the formed tight contact of the two layers at high temperature annealing process constrains the perovskite contraction during they cooling back to room temperature, introducing tensile strain along the in-plane direction and compressive strain along the out-of-plane simultaneously.[1] The strain, ε, can be calculated from the crystal plane spacing according to Equation S2,[2]

$$\varepsilon = \frac{d_{strain\ (hkl)} - d_{non-strain\ (hkl)}}{d_{non-strain\ (hkl)}} \qquad \text{Equation S2}$$

where $d_{\text{non-strain (hkl)}}$ is the non-strained crystal plane spacing of the freestanding perovskite powders, $d_{\text{strain (hkl)}}$ is the strained crystal plane spacing of the perovskite film. The compressive strain along the out-of-plane direction is negative, and the tensile strain along the in-plane direction is positive based on the strain equation. Then, the stress, σ, can be calculated from the obtained strain values according to Hooke's law Equation S3,

$$\sigma = E_p\, \varepsilon \qquad \text{Equation S3}$$

where E_p is the modulus of the perovskite.

We calculated the out-of-plane strain variation on the pristine and PTG prepared $CsPbI_2Br$ films (Fig. S9). After PTG treatment, the compressive strain along the out-of-plane direction in the $CsPbI_2Br$ film dramatically decreases from -0.61×10^{-2} to -0.21×10^{-2}. In addition, to evaluate the correctness of this strain value, we have performed in-plane XRD measurement on the pristine and PTG prepared $CsPbI_2Br$ films to measure the spacing of the planes in parallel to the substrate (Fig. 3). The results show that after PTG

treatment, the tensile strain of the $CsPbI_2Br$ film in the horizontal direction dramatically decreases from $1.62\pm0.05 \times 10^{-2}$ to $0.62\pm0.02 \times 10^{-2}$ (Table S2).

According to the previous reports,[3-5] if there is a tensile strain in perovskite film along the in-plane direction, the direction perpendicular to the substrate would be under the compressive strain simultaneously, and vice versa. Moreover, ε_x and ε_y are linearly related ($\varepsilon_y = -\upsilon\varepsilon_x$, where ε_y is compressive strain of the out-of-plane, ε_x is tensile strain of the in-plane, and υ is Poisson's ratio). Based on the experimental results of compressive strain and tensile strain, the obtained ν values are between 0.37 and 0.29 (Table S1), which is close to the value of perovskites reported in previous papers,[6, 7] demonstrating the rationality of the strain model.

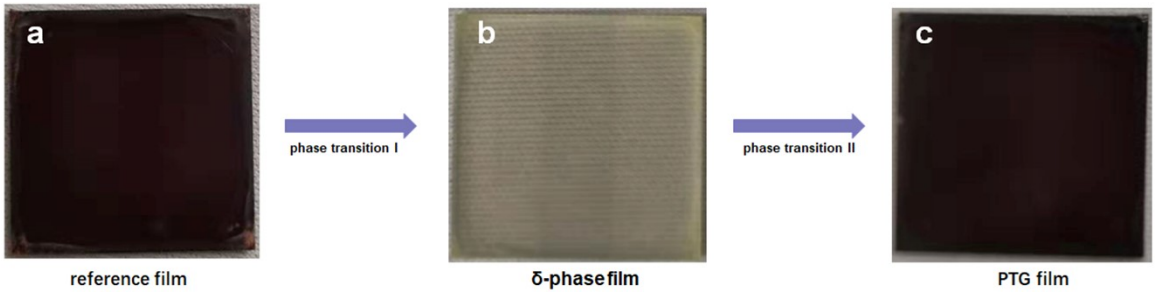

Fig. S1 Optical images of (a) reference film, (b) the δ-phase film, and (c) the PTG film, respectively.

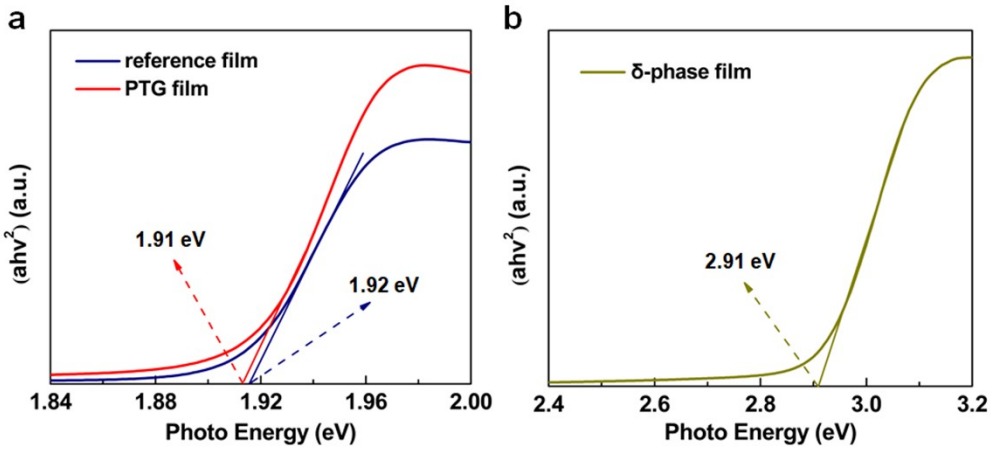

Fig. S2 The bandgap of the three films calculated from UV-vis spectra.

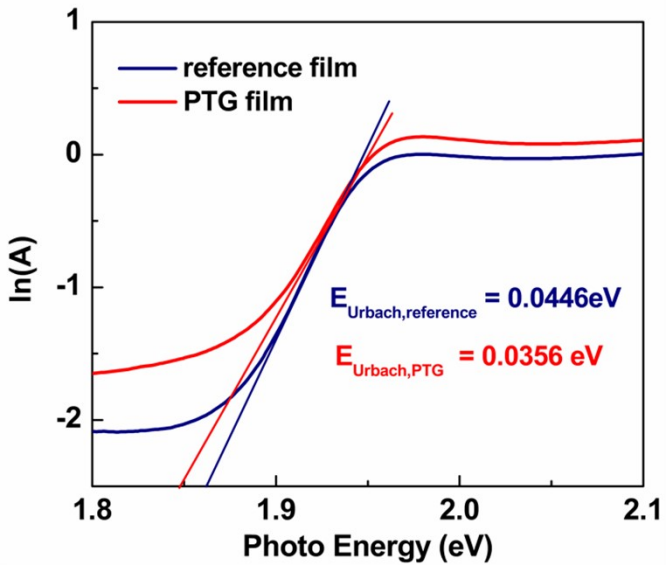

Fig. S3 The Urbach energy of the reference film and the PTG film.

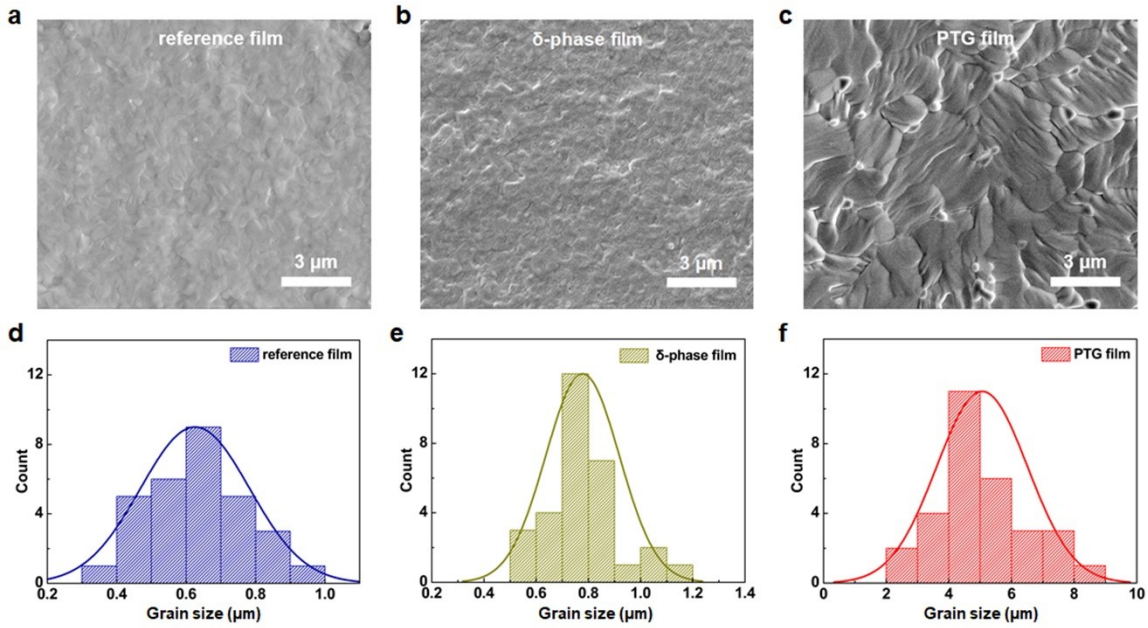

Fig. S4 Top-view SEM images of three films, and corresponding grain size distribution histograms.

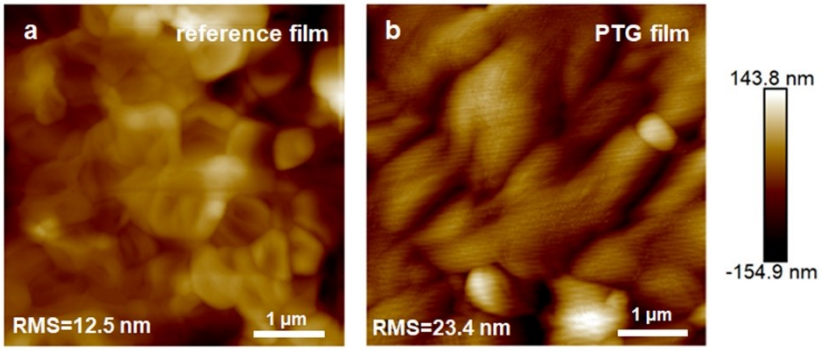

Fig. S5 AFM images of (a) the reference film and (b) the PTG film.

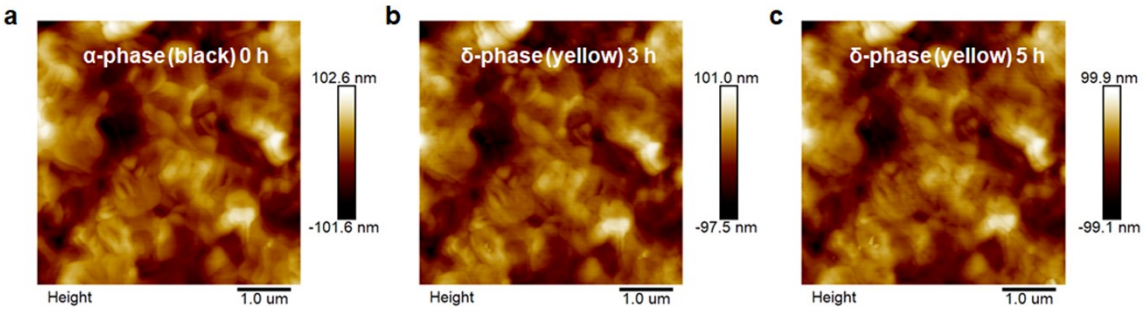

Fig. S6 In-situ AFM images of the reference film over time at 45-50% RH.

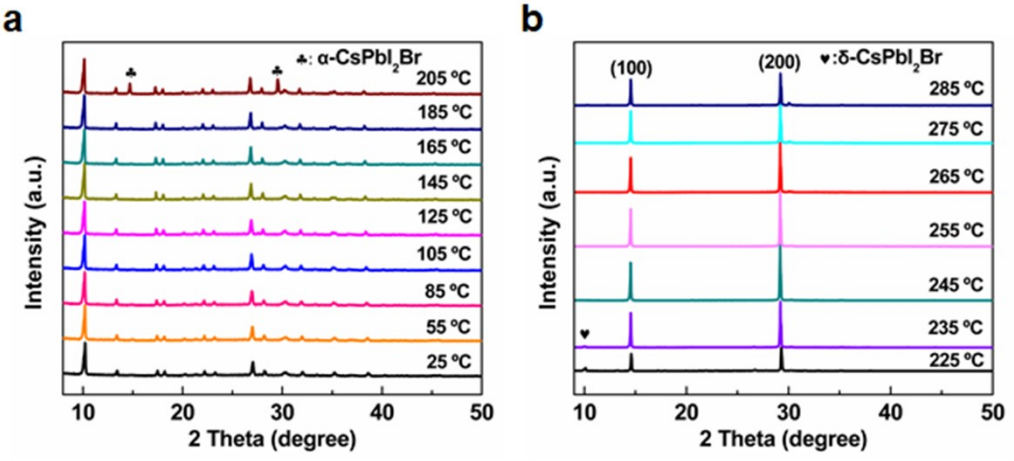

Fig. S7 (a-b) In-suit dynamic XRD patterns of δ-phase $CsPbI_2Br$ film.

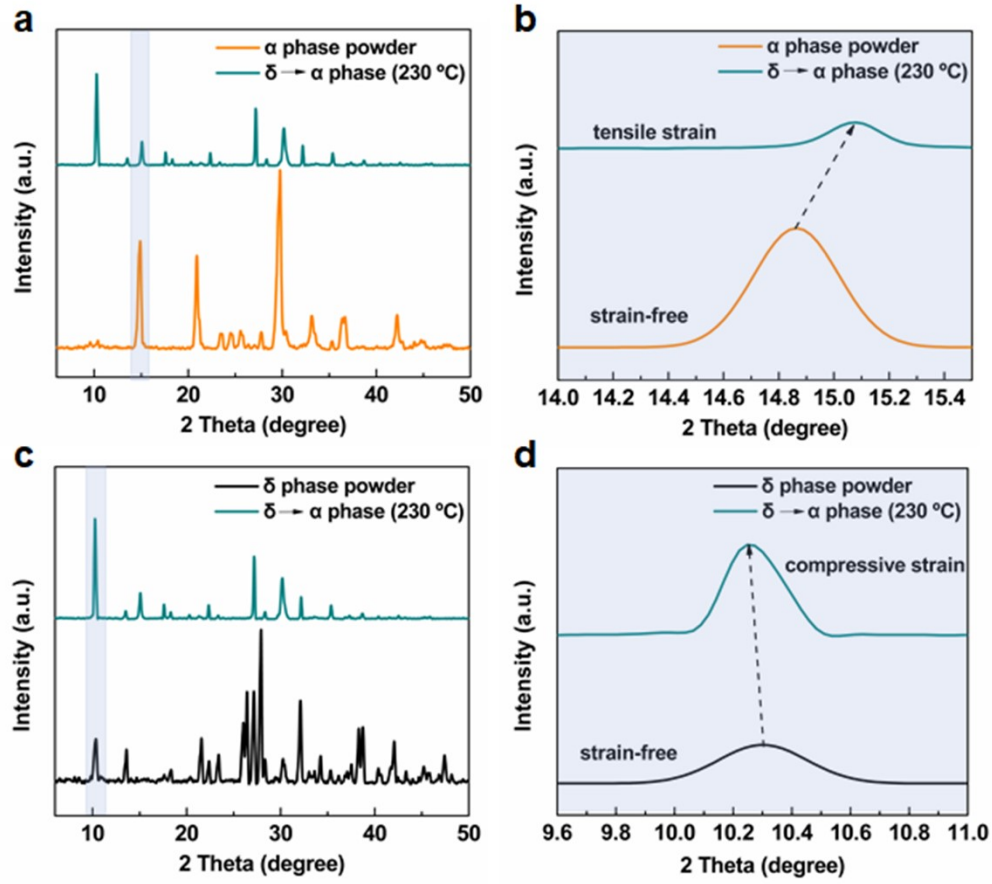

Fig. S8 (a) Out-of-plane XRD patterns of α phase powder scraped from $CsPbI_2Br$ thin film and PTG film formed at 230 ℃. (b) Magnified (100) diffraction peaks of PTG film in the region indicated by the blue color. (c) Out-of-plane XRD patterns of δ phase powder scraped from $CsPbI_2Br$ thin film and PTG film formed at 230 ℃. (d) Magnified diffraction peaks of PTG film in the region indicated by the blue color. At the beginning of δ→α phase transition period, a high tensile strain is observed in α phase $CsPbI_2Br$. Meanwhile, a high compressive strain is observed in δ phase $CsPbI_2Br$. The compressive strain in the δ phase $CsPbI_2Br$ might be the reason causing the high tensile strain in α phase $CsPbI_2Br$.

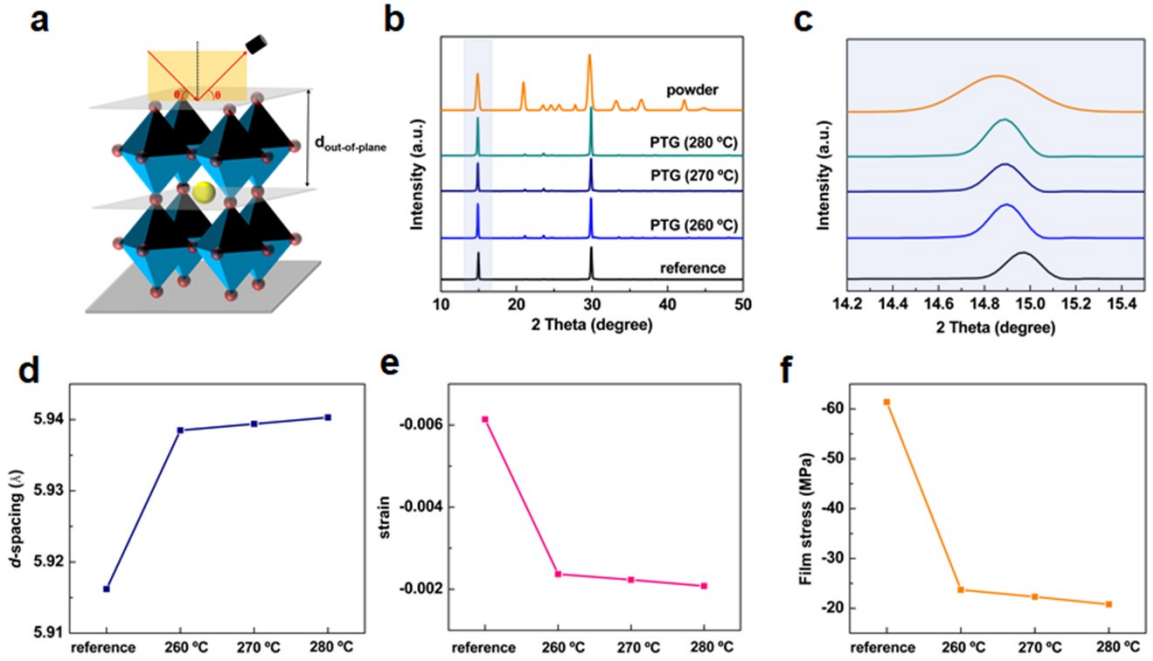

Fig. S9 (a) Schematic illustration of out-of-plane XRD characterization. (b) XRD patterns of the reference film, powder scraped from $CsPbI_2Br$ thin film, and PTG film formed at different temperatures. (c) Magnified (100) diffraction peaks in the region indicated by the blue color. (d) Calculated (100) d-spacing of the different $CsPbI_2Br$ film. (e) Calculated strain in $CsPbI_2Br$ films in the direction perpendicular to the substrate. (f) Calculated stress in $CsPbI_2Br$ films in the direction perpendicular to the substrate.

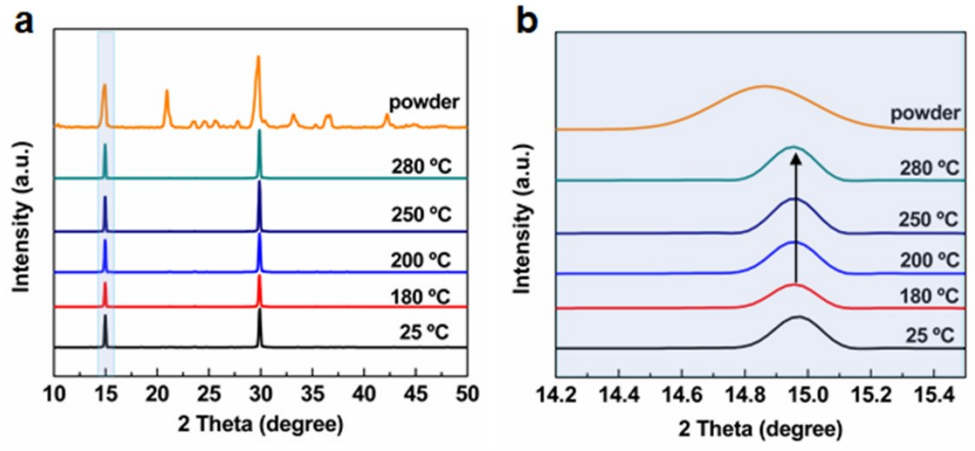

Fig. S10 (a) Out-of-plane XRD patterns of powder and the reference film reheated at different temperatures. (b) Magnified (100) diffraction peaks of PTG film in the region indicated by the blue color.

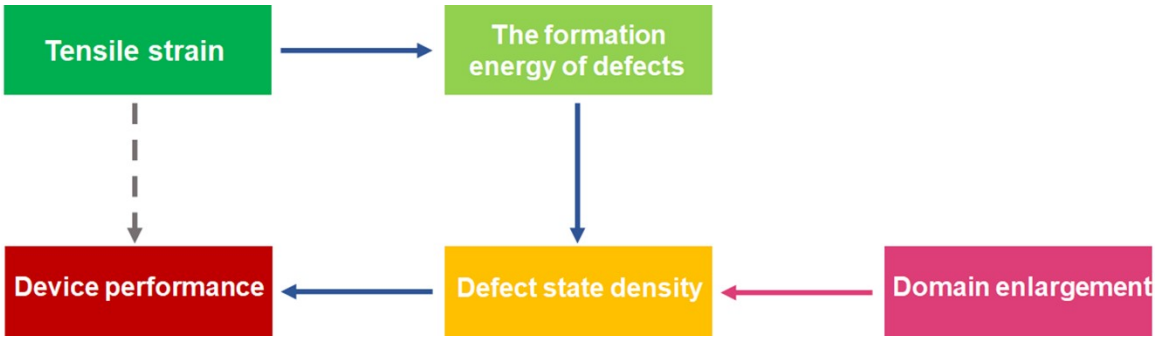

Fig. S11 Schematic diagram of strain affecting device performance.

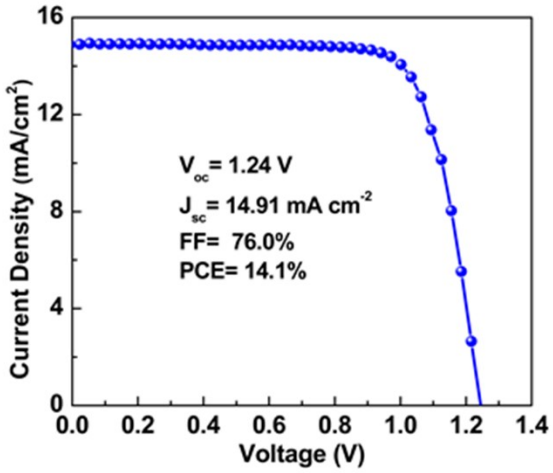

Fig. S12 Typical *J*-V curves of device based on the reference film reheated at 280 ℃.

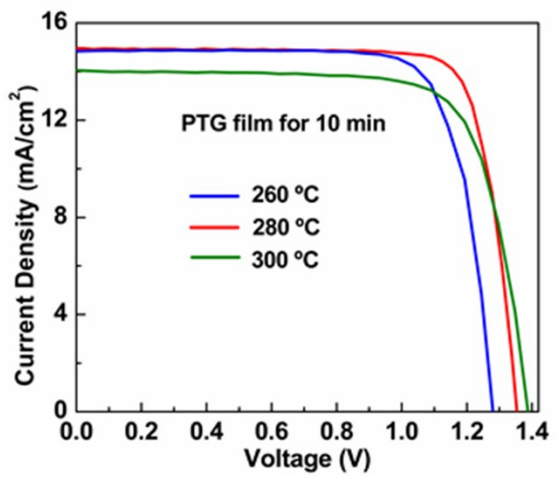

Fig. S13 Typical J-V curves of devices based on the PTG film formed at different temperature.

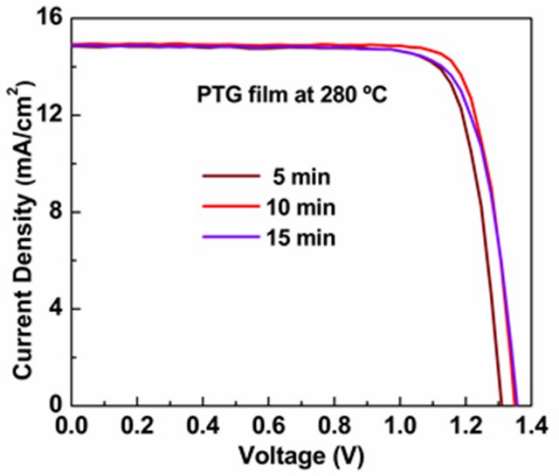

Fig. S14 Typical J-V curves of devices based on the PTG film annealed for different time.

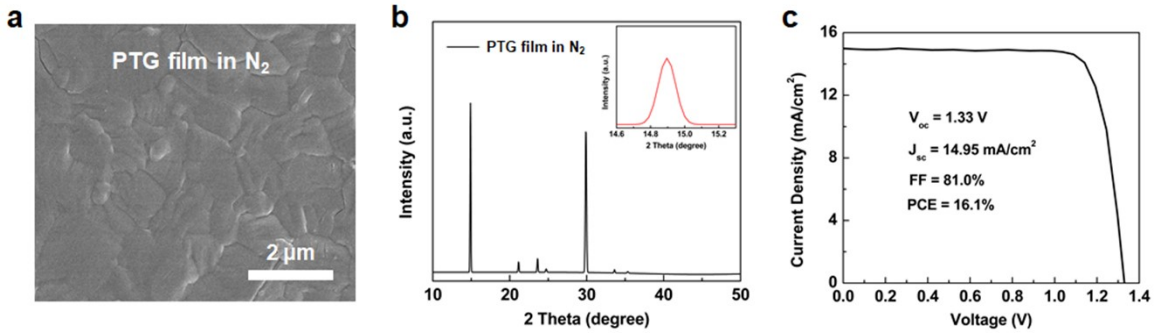

Fig. S15 (a) Top-view SEM image of the PTG film in N_2. (b) XRD patterns and magnified (100) diffraction peak shown in the inset. (c) J-V curve of the PTG device in N_2.

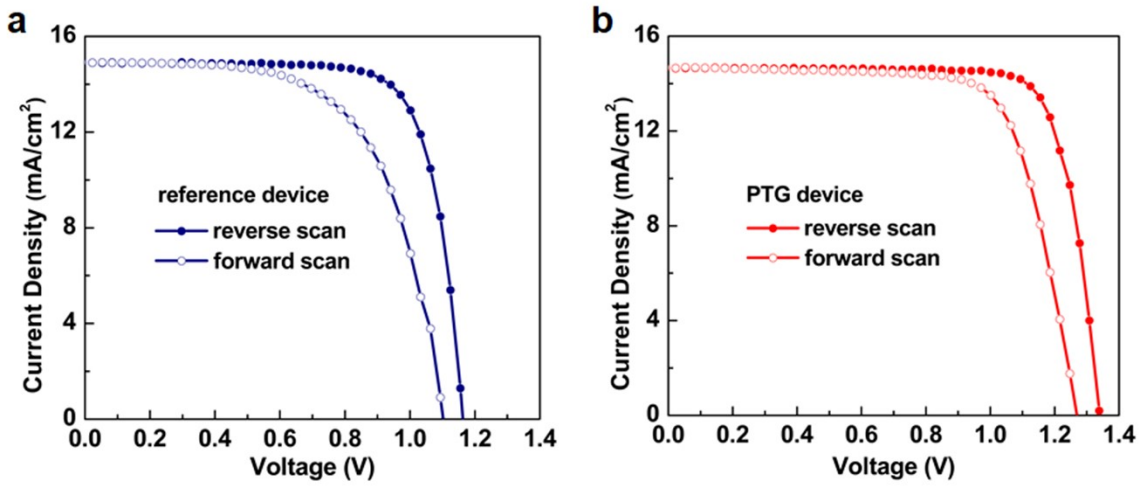

Fig. S16 Typical J-V curves of the reference device and the PTG device with reverse and forward scan, respectively.

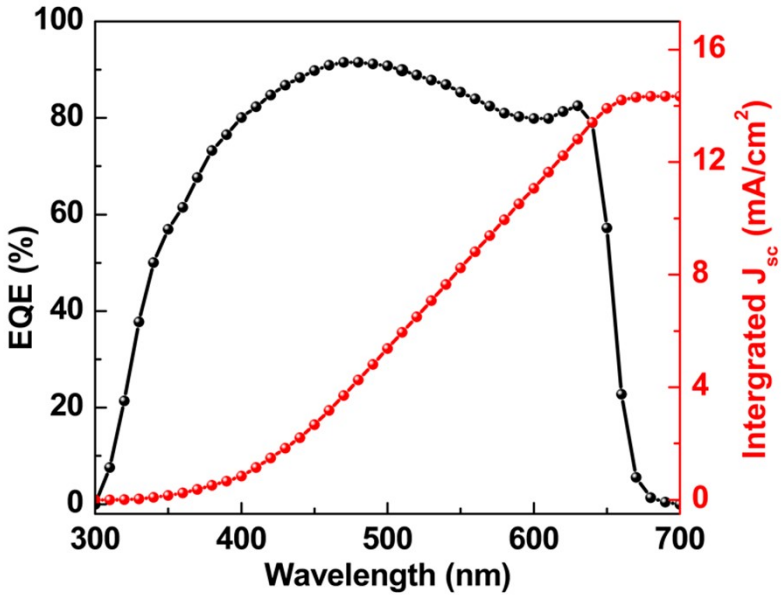

Fig. S17 EQE spectrum and integrated J_{sc} of the PTG device.

Table S1 A summary of the detail strain along out-of-plane direction and along in-plane direction for different $CsPbI_2Br$ film, and corresponding Poisson's ratio.

	Strain along out-of-plane direction ε_y	Strain along in-plane direction ε_x	Poisson's ratio (υ)	Average of Poisson's ratio (ν_{ave})
reference film	-0.006139	0.01641	0.3741	0.33±0.03
PTG film (260℃)	-0.002371	0.008071	0.2938	
PTG film (270℃)	-0.002231	0.006854	0.3255	
PTG film (280℃)	-0.002081	0.006201	0.3356	

Table S2 A summary of the detail strain along in-plane direction for the reference films and PTG films (280 ℃).

Films	2θ (°)	d spacing (Å)	Strain along in-plane direction ε_x	Average (ε_x)	Relaxation of the relative tensile strain (η)
Reference	14.628	6.0503	0.01641	0.0162±0.0005	62±4%
	14.625	6.0519	0.01666		
	14.630	6.0450	0.01551		
PTG	14.777	5.9898	0.006201	0.0062±0.0002	
	14.781	5.9883	0.005980		
	14.775	5.9907	0.006384		

Table S3 PL carrier lifetimes extracted from PL decay measurements.

	A_1	τ_1	A_2	τ_2	τ_{ave}
reference film	0.58	24.98	0.42	96.08	77.30
PTG film	0.55	49.76	0.45	165.53	131.52

Table S4 Photovoltaic performance parameters for two devices.

Device	V_{oc} (V)	J_{sc} (mA/cm^{-2})	FF (%)	PCE (%)
reference	1.14	14.91	79.0	13.4
	(1.11±0.02)	(14.87±0.04)	(78.2±0.9)	(12.9±0.3)
PTG	1.36	14.99	81.1	16.5
	(1.33±0.02)	(14.94±0.06)	(79.9±0.8)	(15.9±0.3)

Table S5 A summary of the detail performance parameters of reported $CsPbI_2Br$ PSCs

Device structure	Bandgap (eV)	Voltage (V)	E_{loss} (V)	Efficiency (%)	Refs
ITO/SnO_2/$CsPbI_2Br$/P3HT/Au	**1.91**	**1.36**	**0.55**	**16.5**	**This work**
FTO/c-TiO_2/$CsPbI_2Br$/Spiro-MeOTAD/Ag	1.92	1.11	0.81	9.84	[8]
FTO/c-TiO_2/$CsPbI_2Br$/Spiro-MeOTAD/Ag	1.90	1.10	0.80	10.34	[9]
FTO/c-TiO_2/$CsPbI_2Br$/Spiro-MeOTAD/Au	1.92	1.23	0.69	10.7	[10]
FTO/c-TiO_2/$CsPbI_2Br$/Spiro-MeOTAD/Ag	1.90	1.13	0.77	10.5	[11]
ITO/c-TiO_2/$CsPbI_2Br$/Spiro-MeOTAD/Au	1.92	1.05	0.87	9.08	[12]
ITO/SnO_2/$CsPbI_2Br$/Spiro-MeOTAD/Au	1.90	1.10	0.80	10.99	[13]
FTO/SnO_2/$CsPbI_2Br$/Spiro-MeOTAD/Ag	1.91	1.29	0.62	12.34	[14]
ITO/SnO_2/$CsPbI_2Br$/Spiro-MeOTAD/Au	1.92	1.22	0.70	14.21	[15]
ITO/SnO_2/ZnO/$CsPbI_2Br$/Spiro-MeOTAD/MoO_3/Ag	1.92	1.23	0.69	14.6	[16]
FTO/c-TiO_2/$CsPbI_2Br$/$CsPbX_3$/PTAA/Au	1.91	1.22	0.69	14.81	[17]
ITO/c-TiO_2/$CsPbI_2Br$/Spiro-MeOTAD/Au	1.92	1.23	0.69	16.07	[18]
FTO/NiOx/ln-$CsPbI_2Br$/ZnO@C_{60}/Ag	1.92	1.15	0.77	13.57	[19]
ITO/SnO_2/$CsPbI_2Br$/Spiro-MeOTAD/Ag	1.91	1.23	0.68	14.15	[20]
ITO/ETL/$CsPbI_2Br$/PDCBT/MoO_3/Ag	1.92	1.30	0.62	16.2	[21]
FTO/c-TiO_2/m-TiO_2/$CsPbI_2Br$/HTL/Au	1.92	1.31	0.61	14.86	[22]
ITO/SnO_2/$CsPbI_2Br$/Spiro-MeOTAD/Au	1.92	1.32	0.60	15.5	[23]
FTO/c-TiO_2/$CsPbI_2Br$/P3HT/Au	1.90	1.01	0.89	7.7	[24]
ITO/TiO_2/$CsPbI_2Br$ NC/P3HT/Au	1.82	1.31	0.50	12.02	[25]
ITO/SnO_2/$CsPbI_2Br$/P3HT/Ag	1.91	1.14	0.77	12.22	[26]
FTO/c-TiO_2/m-TiO_2/$CsPbI_2Br$/P3HT/Au	1.90	0.96	0.94	7.7	[27]
FTO/TiO_2/ $CsPbI_2Br$/Spiro-MeOTAD/Au	1.91	1.30	0.61	15.56	[28]
FTO/TiO_2/$CsPbI_2Br$ /PCBM/Ag	1.88	1.18	0.70	13.6	[29]
ITO/SnO_2/$CsPbI_2Br$/P3HT/Au	1.92	1.185	0.735	13.91	[30]
FTO/TiO_2/$CsPbI_2Br$/Spiro-MeOTAD/Au	1.91	1.25	0.66	15.25	[31]
ITO/ZnO/$CsPbI_2Br$/Spiro-MeOTAD/Ag	1.91	1.21	0.70	14.78	[32]
ITO/SnO_2/$CsPbI_2Br$/poly(DTSTPD-rBThTPD)/Au	1.91	1.41	0.50	15.53	[33]
ITO/SnO_2/$CsPbI_2Br$/$CsPbI_2Br$ /PDTDT/Au	1.91	1.42	0.49	17.36	[34]

References

1 D.-J. Xue, Y. Hou, S.-C. Liu, M. Wei, B. Chen, Z. Huang, Z. Li, B. Sun, A. H. Proppe and Y. Dong, *Nat. Commun.*, 2020, **11**, 1514.

2 J. Zhao, Y. Deng, H. Wei, X. Zheng, Z. Yu, Y. Shao, J. E. Shield and J. Huang, *Sci. Adv.*, 2017, **3**, eaao5616.

3 C. C. Boyd, R. Cheacharoen, T. Leijtens and M. D. McGehee, *Chem. Rev.*, 2018, **119**, 3418-3451.

4 J. Wu, S.-C. Liu, Z. Li, S. Wang, D.-J. Xue, Y. Lin and J.-S. Hu, *Natl. Sci. Rev.*, 2021, **8**, nwab047.

5 N. Rolston, K. A. Bush, A. D. Printz, A. Gold-Parker, Y. Ding, M. F. Toney, M. D. McGehee and R. H. Dauskardt, *Adv. Energy Mater.*, 2018, **8**, 1802139.

6 S. R. Balestra, J. M. Vicent-Luna, S. Calero, S. Tao and J. A. Anta, *J. Mater. Chem. A*, 2020, **8**, 11824-11836.

7 M. Faghihnasiri, M. Izadifard and M. E. Ghazi, *J. Phys. Chem. C*, 2017, **121**, 27059-27070.

8 R. J. Sutton, G. E. Eperon, L. Miranda, E. S. Parrott, B. A. Kamino, J. B. Patel, M. T. Hörantner, M. B. Johnston, A. A. Haghighirad and D. T. Moore, *Adv. Energy Mater.*, 2016, **6**, 1502458.

9 J. S. Niezgoda, B. J. Foley, A. Z. Chen and J. J. Choi, *ACS Energy Lett.*, 2017, **2**, 1043-1049.

10 J. K. Nam, M. S. Jung, S. U. Chai, Y. J. Choi, D. Kim and J. H. Park, *J. Phys. Chem. Lett.*, 2017, **8**, 2936-2940.

11 Y. Wang, T. Zhang, F. Xu, Y. Li and Y. Zhao, *Sol. RRL*, 2018, **2**, 1700180.

12 S. Mariotti, O. S. Hutter, L. J. Phillips, P. J. Yates, B. Kundu and K. Durose, *ACS Appl. Mater. Interfaces*, 2018, **10**, 3750-3760.

13 Y. Jiang, J. Yuan, Y. Ni, J. Yang, Y. Wang, T. Jiu, M. Yuan and J. Chen, *Joule*, 2018, **2**, 1356-1368.

14 J. Yuan, L. Zhang, C. Bi, M. Wang and J. Tian, *Sol. RRL*, 2018, **2**, 1800188.

15 P. Wang, X. Zhang, Y. Zhou, Q. Jiang, Q. Ye, Z. Chu, X. Li, X. Yang, Z. Yin and J. You, *Nat. Commun.*, 2018, **9**, 1-7.

16 L. Yan, Q. Xue, M. Liu, Z. Zhu, J. Tian, Z. Li, Z. Chen, Z. Chen, H. Yan and H. L. Yip, *Adv. Mater.*, 2018, **30**, 1802509.

17 D. Bai, H. Bian, Z. Jin, H. Wang, L. Meng, Q. Wang and S. F. Liu, *Nano Energy*, 2018, **52**, 408-415.

18 W. Chen, H. Chen, G. Xu, R. Xue, S. Wang, Y. Li and Y. Li, *Joule*, 2019, **3**, 191-204.

19 C. Liu, W. Li, H. Li, H. Wang, C. Zhang, Y. Yang, X. Gao, Q. Xue, H. L. Yip and J. Fan, *Adv. Energy Mater.*, 2019, **9**, 1803572.

20 U. Khan, Y. Zhinong, A. A. Khan, A. Zulfiqar and N. Ullah, *Nanoscale Res. Lett.*, 2019, **14**, 116.

21 J. Tian, Q. Xue, X. Tang, Y. Chen, N. Li, Z. Hu, T. Shi, X. Wang, F. Huang and C. J. Brabec, *Adv. Mater.*, 2019, **31**, 1901152.

22 D. H. Kim, J. H. Heo and S. H. Im, *ACS Appl. Mater. Interfaces*, 2019, **11**, 19123-19131.

23 W. Xu, F. He, M. Zhang, P. Nie, S. Zhang, C. Zhao, R. Luo, J. Li, X. Zhang and S. Zhao, *ACS Energy Lett.*, 2019, **4**, 2491-2499.

24 Q. Ma, S. Huang, S. Chen, M. Zhang, C. F. J. Lau, M. N. Lockrey, H. K. Mulmudi, Y. Shan, J. Yao and J. Zheng, *J. Phys. Chem. C*, 2017, **121**, 19642-19649.

25 Q. Zeng, X. Zhang, X. Feng, S. Lu, Z. Chen, X. Yong, S. A. Redfern, H. Wei, H. Wang and H. Shen, *Adv. Mater.*, 2018, **30**, 1705393.

26 Z. Ye, J. Zhou, J. Hou, F. Deng, Y.-Z. Zheng and X. Tao, *Sol. RRL*, 2019, **3**, 1900109.
27 C. F. J. Lau, M. Zhang, X. Deng, J. Zheng, J. Bing, Q. Ma, J. Kim, L. Hu, M. A. Green and S. Huang, *ACS Energy Lett.*, 2017, **2**, 2319-2325.
28. H. Zhao, Y. Han, Z. Xu, C. Duan, S. Yang, S. Yuan, Z. Yang, Z. Liu and S. Liu, *Adv. Energy Mater.*, 2019, **9**, 1902279.
29 H. Sun, J. Zhang, X. Gan, L. Yu, H. Yuan, M. Shang, C. Lu, D. Hou, Z. Hu and Y. Zhu, *Adv. Energy Mater.*, 2019, **9**, 1900896.
30 Z. Wang, A. K. Baranwal, P. Zhang, G. Kapil, T. Ma and S. Hayase, *Nano Energy*, 2019, **66**, 104180.
31 S. Yang, H. Zhao, Y. Han, C. Duan, Z. Liu and S. Liu, *Small*, 2019, **15**, 1904387.
32 J. Ma, J. Su, Z. Lin, L. Zhou, J. He, J. Zhang, S. Liu, J. Chang and Y. Hao, *Nano Energy*, 2020, **67**, 104241.
33 Z. Guo, A. K. Jena, I. Takei, G. M. Kim, M. A. Kamarudin, Y. Sanehira, A. Ishii, Y. Numata, S. Hayase and T. Miyasaka, *J. Am. Chem. Soc.*, 2020, **142**, 9725-9734.
34 Z. Guo, A. K. Jena, I. Takei, M. Ikegami, A. Ishii, Y. Numata, N. Shibayama and T. Miyasaka, *Adv. Funct. Mater.*, 2021, **31**, 2103614.